Precision Engineering 35 (2011) 241–247

Contents lists available at ScienceDirect

Precision Engineering

journal homepage: www.elsevier.com/locate/precision

Low velocity compensation for first order periodic error caused by beam shear

Clay Schluchter[a], Vasishta Ganguly[b], David Chu[a], Tony L. Schmitz[b,*]

[a] Agilent Technologies, Santa Clara, CA, United States
[b] University of Florida, Gainesville, FL, United States

ARTICLE INFO

Article history:
Received 5 February 2010
Received in revised form 31 August 2010
Accepted 23 September 2010
Available online 23 October 2010

Keywords:
Interferometry
Heterodyne
Nonlinearity
Shear

ABSTRACT

This paper describes low velocity first order periodic error compensation caused by beam shear. It is shown that the error compensation is possible using the first order error signal magnitude obtained at high velocity and the interference signal magnitude identified at arbitrarily low velocities. The approach is based on the inverse-proportional relationship between the interference signal and first order periodic error signal magnitudes with variable shear. An experimental setup is described where beam shear is intentionally modified and the first order periodic error is monitored to validate this relationship. A simple compensation algorithm is presented and demonstrated.

1. Introduction

It has been shown recently that the well-known periodic errors caused by frequency leakage in displacement measuring heterodyne interferometers (e.g. [1–4]) can be compensated in real time [5–8]. Periodic error compensation is modeled in rectangular coordinate form with independent sine and cosine magnitude parameters. The magnitudes of these terms are assumed to be stable over at least one millisecond. However, there is no stability assumption for the phase of the sine and cosine terms. The phase is used to update the stage position in real time. The approach is to acquire error parameters, i.e., sine and cosine magnitudes, during target motion in 1 ms intervals and apply the current error parameters through digital compensation in the next millisecond, while again measuring new error parameters. In this way, the compensation is applied in a leap-frog manner with 1 ms latency. While compensation can be applied at any travel velocity, updating the error parameters currently requires that a minimum travel speed be met or exceeded. There are applications, however, where this minimum speed is seldom or never reached in operation. Therefore, the parameters cannot be updated even though they are continuously changing.

An example of this situation is the y-direction interferometer on an x–y lithographic stage used in semiconductor fabrication. The stage makes a series of discrete steps in the y-direction, each with substantial speed. However, each y-direction step is typically followed by a lengthy die exposure scan in the x-direction with low or zero speed in the y-direction. These scans require the highest position accuracy commensurate with the smallest features of the wafer. However, the y-direction interferometer is handicapped by its inability to refresh its cyclic error parameters due to the extremely low speeds.

To avoid beam shear, a plane mirror interferometer rather than a linear interferometer is typically applied. However, beam shear can still be caused during a scan if there are mirror imperfections or the stage is dynamically aligned to keep the local wafer surface normal to the exposure optical axis, for example. In any case, a scenario can exist where compensation for varying first order periodic error due to beam shear at low velocities is desired.

In this work, it is shown that by monitoring the interference signal magnitude, it is possible to compensate first order periodic error even at low velocities. This is based on the inverse-proportional relationship between the interference signal and first order periodic error signal magnitudes. A setup is presented where beam shear is intentionally modified and the first order periodic error is monitored to validate this relationship. A compensation algorithm, verified using a Jones calculus analysis [9], is presented and demonstrated.

2. Experimental setup for intentional beam shear

A schematic of a single pass heterodyne displacement measuring interferometer is provided in Fig. 1. The two light frequencies, f_1 and f_2 ($f_1 > f_2$) are collinear, but orthogonally polarized so that they can be separated at the polarizing beam splitter (PBS). Ideally, f_1 travels only to the moving target and f_2 only to the fixed

* Corresponding author at: University of Florida, Mechanical and Aerospace Engineering, 237 MAE-B, Gainesville, FL 32611, United States. Tel.: +1 352 392 8909; fax: +1 352 392 1071.

0141-6359/$ – see front matter © 2010 Elsevier Inc. All rights reserved.
doi:10.1016/j.precisioneng.2010.09.014

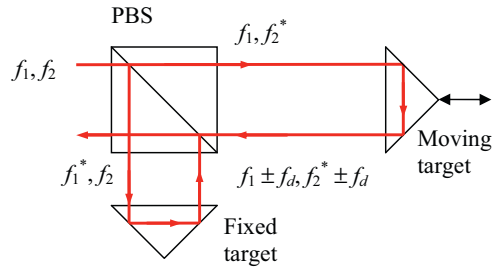

Fig. 1. Schematic of single pass heterodyne interferometer with frequency leakage.

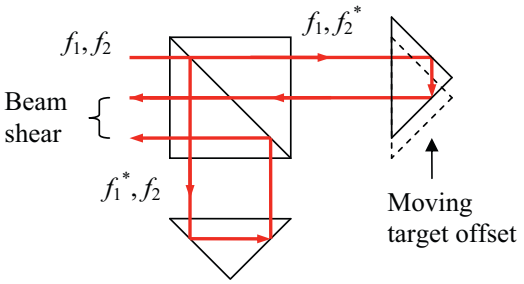

Fig. 2. Beam shear caused by lateral motion of the moving target.

target. However, due to physical imperfections, frequency leakage can occur. Specifically, f_1 and f_2 travel to the both the moving and fixed targets. In this case, rather than obtaining only the intended interference term (composed of f_1 from the moving target Doppler shifted by f_d and f_2 from the fixed target), multiple interference terms appear in the frequency spectrum. These multiple "interferometers" yield the cyclical perturbations in the measurement signal referred to as periodic error. The frequency leakage is depicted in Fig. 1, where an asterisk is used to identify the unintended frequency in each path.

The individual frequencies that appear in the spectrum for the fully leaking interferometer during target motion are: (1) $(f_1 - f_2) \pm f_d$, the intended interference signal, which appears at the beat frequency, $f_b = (f_1 - f_2)$ up or down shifted by the Doppler frequency depending on the motion direction; (2) $(f_1^* - f_2)$ and $(f_1 - f_2^*)$, which are responsible for first order periodic error and appear at f_b; (3) $(f_1^* - f_2^*) \mp f_d$, which is responsible for second order periodic error and is up or down frequency shifted from f_b in the direction opposite to the intended interference signal; and (4) $(f_1 - f_1^*) \pm f_d$ and $(f_2 - f_2^*) \pm f_d$, which are equivalent to homodyne interference signals and are only problematic at high velocities and correspondingly large Doppler shifts[1] [10]. Note that a sufficiently high velocity/Doppler shift is required to isolate the first three signals by frequency.

Beam shear, or a change in overlap between the beams returning from the fixed and moving targets, is introduced by a lateral offset (perpendicular to the motion direction) of the moving target for the system depicted in Fig. 1. This effect is demonstrated in Fig. 2. In this case, the magnitudes of the signals responsible for first order periodic error are unaffected because they exist in a single path. Specifically, both f_1^* and f_2 appear in the fixed path and both f_1 and f_2^* appear in the moving path. However, the magnitudes of the remaining signals do vary with the change in beam overlap. The magnitude of the intended interference signal between f_1 and f_2 varies with beam shear because the overlap between the two (nominally) Gaussian profile beams changes. Similarly, the magnitude of the second order periodic error changes with beam shear because the overlap between f_1^* and f_2^* varies.

Periodic error magnitudes can be calculated using the magnitudes of the individual interference terms [11,12]. First order error depends on the ratio of the magnitudes of the $(f_1^* - f_2)$ and $(f_1 - f_2^*)$ signals to the magnitude of the $(f_1 - f_2) \pm f_d$ signal (intended interference signal). If the magnitude of the $(f_1^* - f_2)$ and $(f_1 - f_2^*)$ signal pair at f_b is taken to be Γ_1 and the magnitude of the intended interference signal is Γ_0, then the maximum first order periodic error magnitude depends on the ratio Γ_1/Γ_0 (see Appendix A). Because Γ_1 is constant, but Γ_0 is not, their ratio varies and first order periodic error magnitude changes with beam shear.[2] For second order periodic error, the maximum magnitude depends on the ratio Γ_2/Γ_0, where Γ_2 is the magnitude of the $(f_1^* - f_2^*) \mp f_d$ term. In this case, both Γ_2 and Γ_0 change by nominally the same amount so their ratio is constant and second order error does not vary appreciably with beam shear.

As noted, however, these error magnitude calculations require that the individual signals can be resolved to the 1 kHz level in the frequency spectrum, which demands target velocities that exceed 158 mm/s (single pass configuration) to achieve the necessary separation via the Doppler shift. In this work, it is shown that low velocity compensation for first order periodic error is possible using the first order error signal magnitude obtained at high velocity and the interference signal magnitude identified at any velocity.

3. Experimental validation

3.1. Test setup

In order to enable variable beam shear in a single pass heterodyne interferometer, a dedicated setup was developed; see Fig. 3. In this setup, a two-frequency laser head (Zeeman frequency split) directed the 1.5 mm diameter, collinear light beams first through an adjustable half wave plate (HWP), which enabled the nominally orthogonal linear polarization vectors to be rotated and change the amount of frequency leakage in the PBS. The beams then passed through a non-polarizing beam splitter (NPBS), where the reference signal for phase measurement was obtained. Next, the two frequencies were nominally separated at the PBS and traveled to the fixed and moving targets; the moving retroreflector (RR) was mounted on an air bearing stage. The beams were recombined in the PBS, turned 90° by a prism, and passed through an adjustable linear polarizer (LP), which enabled the interference signal magnitudes to be modified. This provided the measurement signal for the phase measuring electronics (312.5 kHz sampling frequency, 0.3 nm resolution).

In the setup, the axis of the air bearing stage was first carefully aligned with the beam axis; the alignment was verified by monitoring the magnitude of the interference terms at high velocity along the full stage travel using an analog spectrum analyzer. Beam shear was controlled by adjusting the lateral position of the moving RR using a micrometer cross slide. Tests were conducted by setting the cross slide position for a particular beam offset, collecting the position data using the phase measuring electronics, and then analyzing the data to determine the first and second order periodic error magnitudes. The periodic error magnitudes were identified by: (1) separating the position data time series into multiple sections; (2) subtracting a least squares polynomial fit to remove the local macroscale motion (due to both the position change and non-constant velocity) and isolate periodic error; (3) calculating the

[1] These terms are not considered in this work.

[2] The reader may note that frequency leakage is necessary to induce periodic error, but it is the change in overlap of the signals due to beam shear which causes a variable magnitude for the first order periodic error frequency component.

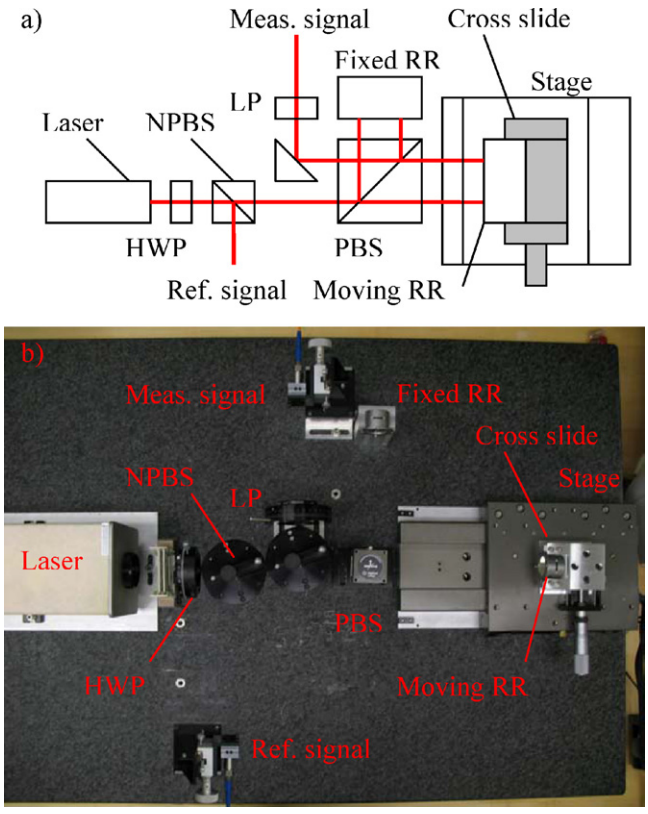

Fig. 3. (a) Schematic of experimental setup to enable adjustable beam shear. (b) Photograph of experimental setup.

discrete Fourier transform of the residual time-domain data; (4) identifying the first and second order periodic error magnitudes based on the Doppler shift (commanded velocity); and (5) averaging the results from the individual sections.

3.2. Experimental results

Fig. 4 demonstrates the variation in signal magnitudes with changes in offset. The HWP and LP angles were 10° from their nominal orientations to introduce significant periodic error content. The data was collected using a spectrum analyzer and the velocity was 5000 mm/min to produce sufficient frequency separation. It is seen that the intended interference signal (up-shifted by 263.3 kHz relative to the 3.6 MHz beat frequency) magnitude varies significantly with offset. It is maximum when the beams from the fixed

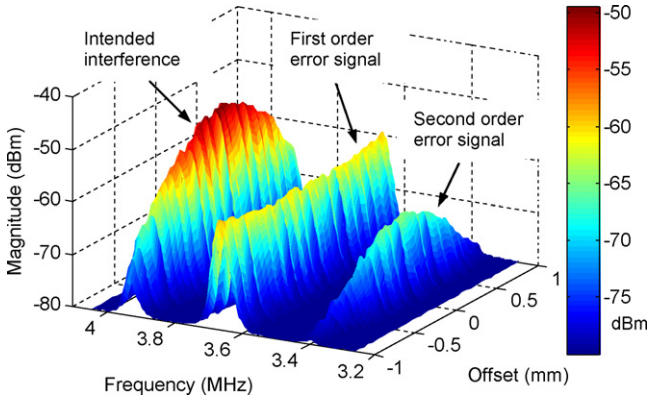

Fig. 4. Variation in signal magnitudes with changes in the moving RR offset (beam shear).

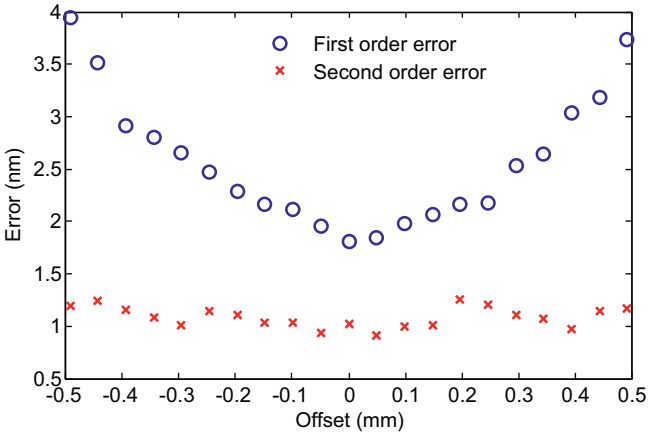

Fig. 5. Variation in periodic error magnitudes versus moving RR offset with 3° HWP and LP misalignments and a velocity of 100 mm/min.

and moving RRs are ideally overlapped (zero offset) and reduces with the moving RR lateral offset in either direction (±1 mm in the plot). The situation is similar with the second order error signal (down-shifted by 263.3 kHz relative to the 3.6 MHz beat frequency) magnitude. However, the magnitude of the first order error signal, which appears at the beat frequency, does not change with offset as discussed previously.

Fig. 5 shows the variation in first and second order periodic error magnitudes with offset. These magnitudes were determined from position data (obtained using the phase measuring electronics) with 3° HWP and LP misalignments and a velocity of 100 mm/min. Fig. 6 shows the results for 5° HWP and LP misalignments. Naturally, the periodic errors are larger for the increased misalignments. In both cases, the expected variation in first order periodic error magnitude with offset is observed. Additionally, the second order error magnitude is approximately constant, as discussed in Section 2.

In order to demonstrate the inverse-proportional relationship between the intended interference signal and first order periodic error magnitudes, the following procedure was completed. First, the magnitudes of the interference signals were measured at offsets from {+0.6 to −0.6} mm using an analog spectrum analyzer. A velocity of 5000 mm/min was used to provide adequate frequency separation and a misalignment angle of 10° was selected for both the HWP and LP to yield large periodic error magnitudes. Second, the first order periodic error magnitude was calculated using the spectrum analyzer data for each offset. The procedure described

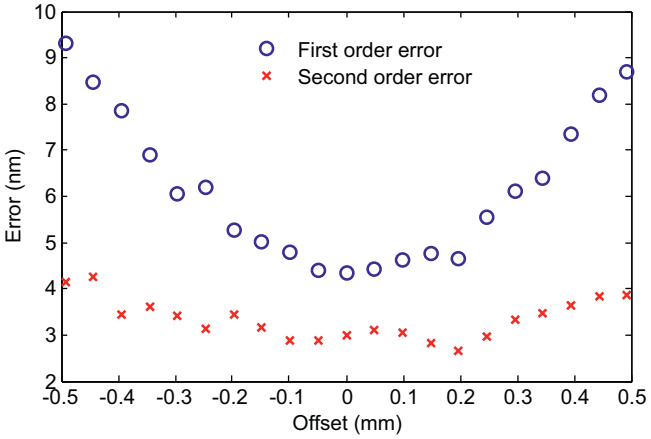

Fig. 6. Variation in periodic error magnitudes versus moving RR offset with 5° HWP and LP misalignments and a velocity of 100 mm/min.

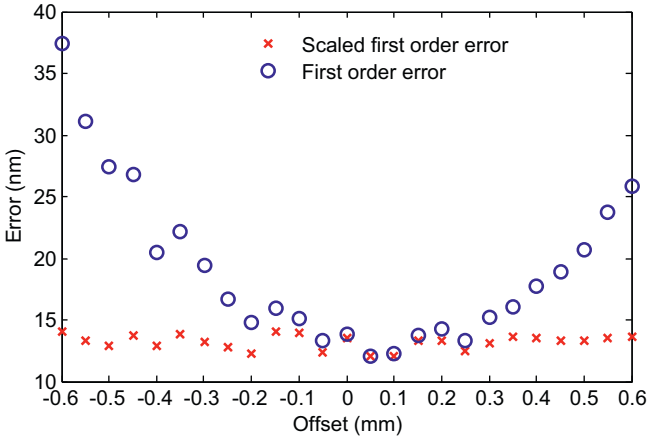

Fig. 7. First order periodic error versus moving RR offset for 10° HWP and LP angles and 5000 mm/min velocity. The scaled error (using Eq. (1)) is also shown.

by Kim and Schmitz [12] was applied. Third, a scaling factor, SF_i, was defined at each offset, i, which depended on the ratio of the intended interference signal magnitude, $\Gamma_{0,i}$ (in dBm), at that offset to the intended interference signal magnitude at zero offset, Γ_0. See Eq. (1), where the power relationships are required to convert from dBm to linear magnitude units. Fourth, the offset-dependent scaling factor was multiplied by the first order periodic error values. The results are displayed in Fig. 7.

$$SF_i = \frac{10^{\Gamma_{0,i}/20}}{10^{\Gamma_0/20}} \tag{1}$$

In Fig. 7 it is seen that the first order periodic error (circles) again follows the parabolic trend observed in the position data analyses from Figs. 5 and 6. The errors are large due to the significant misalignments in the HWP and LP angles. Once the scale factor from Eq. (1) is applied at each offset, however, the scaled first order periodic error (crosses) is approximately constant with offset. This clearly identifies the inverse-proportional relationship between the intended interference signal and first order error magnitudes. Further, it shows that, provided the first order error signal magnitude can be identified (by a high velocity test), monitoring the interference signal magnitude enables the first order periodic error to be compensated, even for low/zero velocity motions.

4. Jones calculus model

In order to analyze the influence of beam shear on periodic error, the following procedure was applied in this study. First, the electric field at the detector was represented in terms of the beam shear and optical frequencies. Next, the resulting interference was expressed as a sum of phasors. Finally, the phase modulation in the intended interference signal caused by each leakage phasor was used to determine the periodic error.

Jones matrices and vectors were applied to describe the leakage field components and interference spectrum. The model used an electric field representation with minimal parameters to describe the effect being studied. Due to the beam offsets, it was necessary to include the spatial magnitude variation of the electric field in at least one dimension (x) transverse to the propagation axis. The phase of each component of the field was determined by the heterodyne optical frequencies, f_1 and f_2, time, t, the wavenumber, k, and roundtrip optical path lengths, M (between the PBS and the moving RR), and R (between the PBS and fixed RR).

Table 1 shows the Jones electric field vectors and optical element matrices that were used in the measurement model. In the table, E_D is the field at the detector; it was obtained by calculating the dot product of the element matrices and the one-dimensional Gaussian profile input beam vector, IB, where ω is the $1/e^2$ waist radius. HWP is the half wave plate element matrix, which includes a rotation angle of ψ about the propagation axis. IF is the interferometer element matrix including an optical path length and beam shear sub element matrix, where x_0 is the beam shear. LP is the linear polarizer matrix with the rotation angle of ϕ about the propagation axis.

Table 1
Jones electric field vectors and optical element matrices.

IB	$4\sqrt{\frac{2}{\pi\omega^2}} \cdot e^{x^2/\omega^2} \begin{pmatrix} e^{i2\pi f_1 t} \\ e^{i2\pi f_2 t} \end{pmatrix}$
HWP	$\begin{pmatrix} \cos(2\psi) & \sin(2\psi) \\ -\sin(2\psi) & \cos(2\psi) \end{pmatrix}$
IF	$\begin{pmatrix} e^{ikM} & 0 \\ 0 & e^{ikR} \end{pmatrix} \begin{pmatrix} e^{x^2/\omega^2} e^{-(x-x_0)^2/\omega^2} & 0 \\ 0 & 1 \end{pmatrix}$
LP	$\frac{1}{2}\begin{pmatrix} 1 & 1 \\ 1 & 1 \end{pmatrix} \cdot \begin{pmatrix} \cos(\phi) & \sin(\phi) \\ -\sin(\phi) & \cos(\phi) \end{pmatrix}$
E_D	LP·IF·HWP·IB

Table 2
Phasor magnitude and frequency for terms in detector power signal.

Term	Magnitude	Frequency
DC	1	0
Signal	$\cos(2\phi)\cos^2(2\psi)e^{-x_0^2/2\omega^2}$	$f_1 - f_2 + \frac{1}{\lambda}\frac{\partial(M-R)}{\partial t}$
First order error	$\sin(2\phi)\sin(4\psi)$	$f_1 - f_2$
Second order error	$\cos(2\phi)\sin^2(2\psi)e^{-x_0^2/2\omega^2}$	$f_1 - f_2 - \frac{1}{\lambda}\frac{\partial(M-R)}{\partial t}$

The resulting linearly polarized field at the detector E_D is given in Eq. (2). This expression was used to determine the power at the detector, P_D, shown in Eq. (3).

$$E_D = \sqrt[4]{\frac{1}{2\pi\omega^2}}(e^{ikR}e^{-x^2/\omega^2}(\sin\phi + \cos\phi)(\cos(2\psi)e^{2i\pi f_2 t} - \sin(2\psi)e^{2i\pi f_1 t}) + e^{ikM}e^{-(x-x_0)^2/\omega^2}(\cos\phi - \sin\phi) \times (\cos(2\psi)e^{2i\pi f_1 t} + \sin(2\psi)e^{2i\pi f_2 t})) \tag{2}$$

$$P_D = \int E_D\overline{E_D}\,\partial x = 1 + e^{-{x_0}^2/2\omega^2}\cos(2\phi)\cos^2(2\psi)\cos(k(M-R) + 2\pi(f_1 - f_2)t) - \sin(4\psi)\sin(2\phi)\cos(2\pi(f_1 - f_2)t) - e^{-{x_0}^2/2\omega^2}\cos(2\phi)\sin^2(2\psi)\cos(-k(M-R) + 2\pi(f_1 - f_2)t) \tag{3}$$

As seen in Eq. (3), the power at the detector was calculated by integrating the intensity; four important terms were obtained. These terms are identified in Table 2 as DC, signal, first order error, and second order error. Note that the second order error is Doppler-shifted in the opposite direction from the signal relative to the beat frequency ($f_1 - f_2$).

The optical power at the detector, P_D, can be interpreted as the sum of phasors. In general, the sum of two phasors can be combined using a magnitude and phase representation. The sum of a first phasor with magnitude A_1 and phase θ_1 and a second phasor with magnitude A_2 and phase $\theta_1 + \Delta\theta$ is given in Eq. (4). If A_2 is much small than A_1, then the resultant is nearly equal to the first phasor with a corresponding small amplitude and phase modulation.

$$A_1\cos(\theta_1) + A_2\cos(\theta_1 + \Delta\theta) = \sqrt{(A_1 + A_2\cos(\Delta\theta))^2 + A_2^2\sin^2(\Delta\theta)}\cos\left(\theta_1 + \tan^{-1}\left(\frac{A_2\sin(\Delta\theta)}{A_1 + A_2\cos(\Delta\theta)}\right)\right) \tag{4}$$

The phasor sum of the first order error and Signal terms yields the first order periodic phase measurement error expression provided in Eq. (5). This expression was expanded using a power series assuming small ψ and ϕ; see Eq. (6).

$$\tan^{-1}\left(\frac{\sin(2\phi)\sin(4\psi)\sin(k(M-R))}{e^{-x_0{}^2/2\omega^2}\cos(2\phi)\cos^2(2\psi)-\sin(2\phi)\sin(4\psi)\cos(k(M-R))}\right) \quad (5)$$

$$\cong \frac{8\,\phi\,\psi}{e^{-x_0{}^2/2\omega^2}}\sin(k(M-R)) \equiv \varepsilon_{FO}\sin(k(M-R)) \quad (6)$$

The phasor sum of the second order error and signal terms produces the second order periodic phase measurement error expression given in Eq. (7). This expression was also expanded using a power series assuming small ψ; see Eq. (8).

$$\tan^{-1}\left(\frac{\sin^2(2\psi)\sin(2k(M-R))}{\cos^2(2\psi)-\sin^2(2\psi)\cos(2k(M-R))}\right) \quad (7)$$

$$\cong 4\psi^2\sin(2k(M-R)) \equiv \varepsilon_{SO}\sin(2k(M-R)) \quad (8)$$

In Eqs. (7) and (8) the first and second order periodic phase measurement error magnitudes are defined as ε_{FO} and ε_{SO}, respectively. Under conditions where the HWP and LP angles, ψ and ϕ, are relatively stable, these errors can be monitored at high velocity (to provide adequate frequency separation) and approximated for low velocity compensation.

5. Compensation approach

It is proposed that some applications would benefit from a first order periodic error compensation at low velocities that is based on the interference signal magnitude, *SM*. This signal magnitude appears in the denominator of the expression for ε_{FO} (Eq. (6)). The form of the compensation can be expressed as shown in Eq. (9), where x_{1s} and x_{1c} are the magnitudes of the first order sine and cosine periodic error signals. Because this is a first order error the argument of the sine and cosine functions is simply the position signal, p.

$$\frac{x_{1s}}{SM}\sin(p)+\frac{x_{1c}}{SM}\cos(p) \quad (9)$$

As described in Section 2, the second order periodic error is not influenced by beam shear so *SM* should not be used in the compensation. The argument of the sine and cosine is now twice the position signal; see Eq. (10).

$$x_{2s}\sin(2p)+x_{2c}\cos(2p) \quad (10)$$

The leapfrog periodic error compensation method [5–8] with beam shear compensation was simulated using experimental position data. The data was acquired with the HWP and LP angles set to 10° from their nominal orientations at a stage velocity of 100 mm/min. The RR offset was varied from −0.5 mm to 0.5 mm. For the experimental setup, the corresponding beam shear was twice the RR offset (see Fig. 2). Because these settings were used to help isolate and increase the periodic error above the noise, the results are not representative of optimized systems. Optimized systems will achieve much lower periodic errors and filtering can be implemented to further reduce noise.

For the 100 mm/min stage motion, the velocity was high enough to isolate the periodic errors so the data was processed in four ways as shown in Fig. 8, where each curve is the standard deviation, σ, of the data set. Since signals with larger uncompensated periodic error will have larger standard deviations, this metric was selected to compare compensation results. All data have the second order least squares fit macroscale position information removed in 1 ms time segments throughout the travel to isolate periodic error.

In Fig. 8 the top curve (circles) is the signal without compensation. The curve with cross markers is the signal after compensation

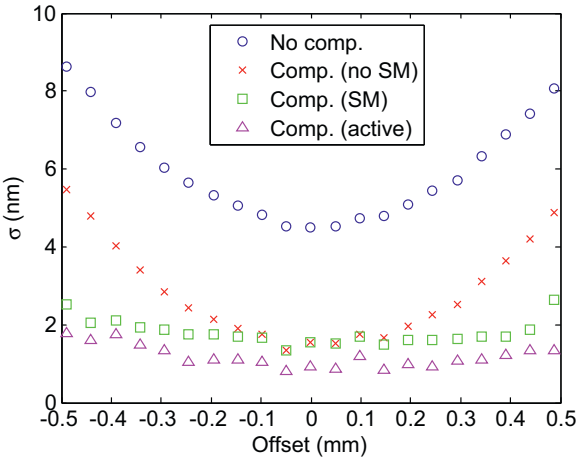

Fig. 8. Standard deviations, σ, of position signal versus moving RR offset (second order least squares fit position information removed): (circle) no compensation; (cross) compensated signal without *SM* updates; (square) compensated signal with *SM* updates; (triangle) compensated signal with active updates at 1 ms intervals.

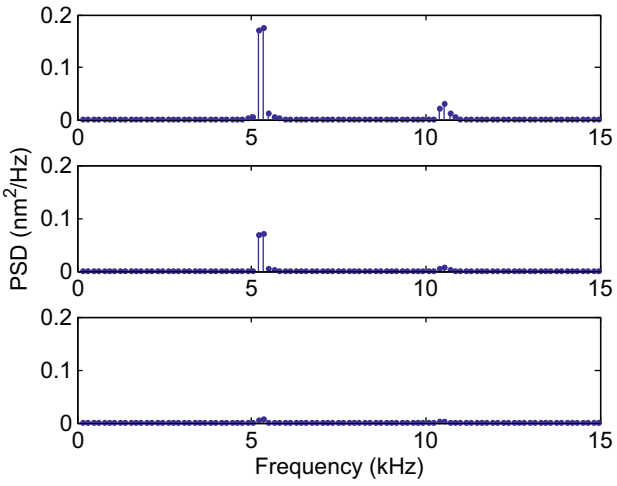

Fig. 9. Power spectral density (PSD) of position signal error at extreme stage position: (top) no compensation; (middle) compensated signal without *SM* updates; (bottom) compensated signal with *SM* updates.

without *SM* updates. This periodic error compensation magnitude was evaluated from 1 ms of data near the center of travel and then applied equally across the data without modifications due to beam shear or signal variation. The curve with square markers is the signal after compensation according to Eq. (9) with *SM* updates. The bottom curve (triangles) is the signal after compensation with active updates at 1 ms intervals throughout the travel. Since the periodic error in this signal is believed to have been compensated accurately, this curve represents an estimate of other noise in the system.

The error spectra in Fig. 9 show the effect of the compensation for the largest experimental beam shear (i.e., the largest offset in Fig. 8). The top panel gives the spectrum of the data with second order least squares fit position information subtracted and no compensation. The middle panel shows the spectrum of the data after compensation without *SM* updates. The bottom panel gives the spectrum of the data after compensation with *SM* updates.

6. Discussion

The required measurement accuracy for the signal magnitude, *SM*, used for compensation in Section 5 was investigated. Because

the first order compensation is nearly inversely proportional to *SM* (as shown in Fig. 7), the residual error (or periodic measurement error remaining after compensation) can be expressed as shown in Eq. (11). This equation emphasizes the role of the *SM* measurement accuracy.

$$\cong -\frac{\partial \varepsilon_{FO}}{\partial SM} = \varepsilon_{FO}\frac{\Delta SM}{SM} \tag{11}$$

If the periodic error in the uncompensated signal is not too large with respect to the allowable residual error budget, then the required accuracy in the *SM* estimate is low. For example, if the raw signal contains 1 nm of periodic error and the residual error must be <0.1 nm, then *SM* must be estimated within 10%.

The improvement of this compensation with respect to compensation without low velocity *SM* updates was also evaluated. The beam shear modification is naturally more important for large shear. If the periodic error magnitude is small, or the low velocity beam shear is small, then the improvement will also be small. In any case, if the beam shears from x_0 to $x_0 + \delta x$, and compensation is applied without *SM* updates, a residual error will result. The lowest order term of the residual error using a power series expansion for small δx is shown in Eq. (12).

$$\begin{aligned}
&\frac{8\phi\psi}{e^{-(x_0+\delta x)^2/2\omega^2}}\sin(k(M-R)) - \frac{8\phi\psi}{e^{-{x_0}^2/2\omega^2}}\sin(k(M-R)) \\
&= \left(\frac{e^{-{x_0}^2/2\omega^2}}{e^{-(x_0+\delta x)^2/2\omega^2}} - 1\right)\frac{8\phi\psi}{e^{-{x_0}^2/2\omega^2}}\sin(k(M-R)) \\
&\cong \frac{x_0\,\delta x}{\omega^2}\frac{8\phi\psi}{e^{-{x_0}^2/2\omega^2}}\sin(k(M-R)) = \frac{x_0}{\omega}\frac{\delta x}{\omega}\varepsilon_{FO}\sin(k(M-R))
\end{aligned} \tag{12}$$

For example, in a system with 10 nm first order periodic phase measurement error magnitude prior to a beam shear from 1.0 to 0.9 times the $1/e^2$ beam radius, then the first order periodic error magnitude will change from 10 nm to roughly 9 nm according to Eq. (12). In this case, $(x_0/\omega) = 1.0$, $(\delta x/\omega) = 0.1$ and $\varepsilon_{FO} = 10$ nm. A system applying compensation without low velocity *SM* updates would apply a 10 nm compensation to a signal with 9 nm periodic error. The residual error is this case would be $(x_0/\omega)(\delta x/\omega)\varepsilon_{FO} = 1.0 \cdot 0.1 \cdot 10$ nm. However, a system that applied low velocity *SM* updates would automatically eliminate this residual error leading to a 1 nm improvement.

There are two final points of emphasis. First, the data in this study was collected in 100 ms intervals and, therefore, the simulation in Section 5 assumed a time limit of roughly 100 ms between high velocity information and low velocity compensation. The effect of longer periodic error estimate age coupled with, for example, variations in laser power and detector gain, or other drifts, was not investigated. However, the time limit of 100 ms is not significant for lithographic applications with, for example, a 1 m/s wafer stage scan velocity, approximately 150 mm reticle dimension, and 4× projection lens magnification. These parameters yield a scan time of 37.5 ms between step motions. Applications that require time periods longer than 100 ms between high velocity compensation updates may not achieve the same improvement shown here. Second, the effects of non-planar wavefronts were not considered here. Depending on the glass path and beam propagation distance, non-planar wavefronts can also lead to variations in the interference signal magnitude. However, it is believed that the proposed algorithm would also work with tilted wavefronts at low velocity, for example. Tilting wavefronts reduces contrast in the intended interference signal without reducing the magnitude of the leakage-induced first order signals so the compensation should still be effective. Further, the magnitude of the second order leakage signal would be reduced at the same rate as the intended signal, so the second order periodic error parameters would again not be updated when the contrast varies.

7. Conclusions

While periodic error can be actively compensated in signals that result from sufficiently high Doppler frequency shifts, it is challenging to compensate periodic errors at low velocity. In systems with stable periodic error sources, it was shown here that low velocity periodic error can be compensated using information obtained from measurements at high velocity. This correction should include the influence from beam shear which can be estimated from the signal magnitude. The data and simulation presented in this study show that this compensation approach offers improved performance for large beam shear and short time durations between high velocity updates.

Appendix A.

The derivation for calculating the first order periodic error is presented here. The corresponding phase error, $\Delta\phi$, expressed in Unit Intervals (UI), where 1 UI = 2π radians, is related to the ratio $r = (\Gamma_1/\Gamma_0)$ as:

$$2\pi \cdot \Delta\phi = \tan^{-1}\left(\frac{r \cdot \sin(2\pi(\phi-\theta))}{1 + r \cdot \cos(2\pi(\phi-\theta))}\right), \tag{A1}$$

where the phases of Γ_0, ϕ, and Γ_1, θ, are also expressed in UI. Note that $\phi = 2s/\lambda$, where s is the ideal position and λ is the wavelength for the single pass interferometer. Also, $\Delta\phi = 2\Delta s/\lambda$, where Δs is the first order periodic error.

To determine the maximum value of Eq. (A1), the partial derivative with respect to the phase difference $(\phi - \theta)$ may be calculated and set to zero. To simplify notation, let $x = (\phi - \theta)$ as shown in Eq. (A2).

$$2\pi\frac{d\Delta\phi}{dx} = \frac{d}{dx}\tan^{-1}\left(\frac{r \cdot \sin(2\pi x)}{1 + r \cdot \cos(2\pi x)}\right) = 0 \tag{A2}$$

By applying $(d/dx)\tan^{-1}(u) \equiv (du/dx) \cdot (1/(1+u^2))$ and considering only the (du/dx) term in the right hand side product, Eq. (A3) is obtained.

$$\frac{d}{dx}\left(\frac{r \cdot \sin(2\pi x)}{1 + r \cdot \cos(2\pi x)}\right) = 0 \tag{A3}$$

Expanding Eq. (A3) gives:

$$\frac{(1 + r \cdot \cos(2\pi x)) \cdot (d/dx)(r \cdot \sin(2\pi x)) - (r \cdot \sin(2\pi x)) \cdot (d/dx)(1 + r \cdot \cos(2\pi x))}{(1 + r \cdot \cos(2\pi x))^2} = 0. \tag{A4}$$

Considering only the numerator, Eq. (A5) is obtained.

$$\begin{aligned}
&(1 + r \cdot \cos(2\pi x)) \cdot 2\pi \cdot (r \cdot \cos(2\pi x)) - (r \cdot \sin(2\pi x)) \cdot 2\pi \cdot \\
&(-r \cdot \sin(2\pi x)) = 0
\end{aligned} \tag{A5}$$

Expanding Eq. (A5) gives:

$$\cos(2\pi x) + r \cdot \cos(2\pi x) \cdot \cos(2\pi x) + r \cdot \sin(2\pi x) \cdot \sin(2\pi x) = 0, \tag{A6}$$

which simplifies to $\cos 2\pi x = -r$. This shows that the extreme values of $\Delta\phi$ occur at $\cos(2\pi x) = \cos(2\pi(\phi - \theta)) = -r$. To determine

the maximum phase error, $\Delta\phi_{max}$, $\cos(2\pi(\phi-\theta))$ can be therefore replaced by $-r$ in Eq. (A1). Furthermore, $\sin(2\pi(\phi-\theta))$ can be replaced by $\sqrt{1-r^2}$ using the identity $\cos^2(x)+\sin^2(x)=1$. See Eq. (A7).

$$2\pi\cdot\Delta\phi_{max} = \tan^{-1}\left(\frac{r\cdot\sqrt{1-r^2}}{1+r(-r)}\right) = \tan^{-1}\left(\frac{r}{\sqrt{1-r^2}}\right) = \sin^{-1}(r). \quad \text{(A7)}$$

References

[1] Fedotova G. Analysis of the measurement error of the parameters of mechanical vibrations. Measurement Techniques 1980;23(7):577–80.
[2] Quenelle R. Nonlinearity in interferometric measurements. Hewlett-Packard Journal 1983;34(4):10.
[3] Barash V, Fedotova G. Heterodyne interferometer to measure vibration parameters. Measurement Techniques 1984;27(7):50–1.
[4] Sutton C. Nonlinearity in length measurements using heterodyne laser Michelson interferometry. Journal of Physics E: Scientific Instrumentation 1987;20:1290–2.
[5] Schmitz T, Chu D, Kim HS. First and second order periodic error measurement for non-constant velocity motions. Precision Engineering 2008;33:353–61.
[6] Schmitz T, Chu D, Houck III L. First order periodic error correction: validation for constant and non-constant velocities with variable error magnitudes. Measurement Science and Technology 2006;17:3195–203.
[7] Schmitz T, Houck III L, Chu D, Kalem L. Bench-top setup for validation of real time, digital periodic error correction. Precision Engineering 2006;30:306–13.
[8] Chu D, Ray A. Nonlinearity measurement and correction of metrology data from an interferometer system. In: Proceedings of Fourth *euspen* International Conference. 2004. p. 300–1.
[9] Jones RC. New calculus for the treatment of optical systems. Journal of the Optical Society of America 1941;31:488–93.
[10] Schmitz T, Beckwith J. An investigation of two unexplored periodic error sources in differential-path interferometry. Precision Engineering 2002;27(3):311–22.
[11] Badami V, Patterson S. A frequency domain method for the measurement of nonlinearity in heterodyne interferometry. Precision Engineering 2000;24(1):41–9.
[12] Kim HS, Schmitz T. Periodic error calculation from spectrum analyzer data. Precision Engineering 2010;34:218–30.